Changes in rotation induced by Pleistocene ice masses with stratified analytical Earth models

L. L. A. Vermeersen,[1] A. Fournier,[2] and R. Sabadini

Dipartimento di Scienze della Terra, Sezione Geofisica, Università di Milano, Milano, Italy

Abstract. The rotational response of the Earth to Pleistocene deglaciation is studied by means of a multilayered, viscoelastic Earth model based on the preliminary reference Earth model (PREM). Incompressible viscoelastic deformation is evaluated from a self-compressed initial state. The novelty of our approach stands on the application of a fully analytical normal mode theory to the response of the Earth to surface loads and variations in the centrifugal potential for large numbers of viscoelastic layers, as requested by PREM. Assuming that both present-day true polar wander (TPW) and changes in the second-degree component of the geopotential ($\dot{J}_2$) are solely due to Pleistocene postglacial rebound, we obtain for a two-layer viscosity model that the upper mantle viscosity must be lowered to about $1 - 5 \times 10^{20}$ Pa s with respect to the classical value of 10^{21} Pa s. This upper mantle viscosity is accompanied by an increase of the lower mantle viscosity by a factor of 25, in agreement with some recent relative sealevel (RSL) data analyses and convectively supported long-wavelength geoid anomalies. When the viscosity contrast is located at 1470 km depth, TPW and $\dot{J}_2$ require a viscosity of 10^{21} Pa s in the upper part of the mantle (above 1470 km depth), with a moderate viscosity increase in the lowermost portion of the mantle. This result indicates that a viscosity of 10^{21} Pa s is appropriate for a wider portion of the mantle than the upper mantle, in agreement with *Haskell's* [1935] estimate that was not limited to the seismically inferred 670 km boundary.

1. Introduction

The inference of the viscosity structure of the mantle is a basic issue in geodynamics. A variety of important geodynamical processes, from the long timescale convection in the mantle to the faster response of the Earth to Pleistocene deglaciation, depends on this parameter.

In spite of the efforts made by several authors in the last decades a general consensus on the viscosity profile of the mantle has not been reached yet. The use of two different classes of observables in modeling mantle deformation processes, convection and postglacial rebound, which occur on different timescales, is certainly one of the major causes for the discrepancies among the various inferences of mantle viscosity. It has been suggested that the creep properties of the mantle do

not remain constant at short and long timescales. Convection and postglacial rebound could be controlled by steady state and transient creep, respectively. If this is the case, modeling of postglacial rebound by means of a steady state rheology causes a bias in the inference of viscosity [*Sabadini et al.*, 1985; *Peltier*, 1985]. This point of view has been weakened recently by rebound analyses that show that a number of glacial isostatic adjustment data are consistent with a conspicuous viscosity increase in the lower mantle [*Nakada and Lambeck*, 1989] that is generally found from long-wavelength geoid analyses [*Richards and Hager*, 1984]. Recent papers by *Forte and Mitrovica* [1996] and *Mitrovica and Forte* [1997] reinforce this indication by means of a joint inversion of mantle convection and postglacial rebound data that requires a significant viscosity increase with depth in the mantle.

Estimated viscosity profiles differ substantially from one another, even within the various postglacial rebound analyses. Typically, some studies predict a rather uniform mantle viscosity [*Yuen et al.*, 1986; *Tushingham and Peltier*, 1992; *Spada et al.*, 1992], while other analyses require a substantial viscosity contrast at the interface between the upper and lower mantles [*Lambeck et al.*, 1990]. *Mitrovica* [1996], to whom we refer for an exhaustive discussion on these issues, has

---

[1]Now at Geodetic Institute, Stuttgart University, Stuttgart, Germany.

[2]Now at Departement des Sciences de la Matiere, Ecole Normale Superieure, Lyon, France.

provided a possible explanation for these apparently contradictory results. He suggests that they are consequences of a misinterpretation of the *Haskell* [1935] value, considered limited to the upper mantle after the results of the modern seismology. Other causes of apparent inconsistencies among the various glacial isostatic studies could be ascribed to the use of different Earth models, different observables considered by the various authors, and insufficient search in the parameter space of the rebound models [*Lambeck et al.*, 1996].

This study is a contribution to the clarification of these issues, showing that our previous results based on rotation and J_2 observations may have been biased by simplified Earth models in which, because of the reduced number of (visco)elastic layers with respect to the preliminary reference Earth model (PREM) [*Dziewonski and Anderson*, 1981], the buoyancy has been underestimated.

Benchmark calculations have been carried out with several authors on the various parts of the codes that enter the theory of rotational readjustment to Pleistocene deglaciation. The load and rotational relaxation parts of our models have been benchmarked separately with different groups, which makes us confident that the following results can contribute to clarifying the issues mentioned above.

The observational data considered in our analysis are taken from *Dickman* [1977] and *McCarthy and Luzum* [1996] for true polar wander (TPW), and from *Yoder et al.* [1983] and *Devoti et al.* [1997] for J_2. For a review on how these data have been derived we refer to the introduction of the paper by *Peltier and Jiang* [1996].

Figure 1 is a cartoon showing the secular component of $0.9°$ Myr^{-1} toward Newfoundland of the present-day polar motion, once the Chandler wobble, the yearly and the decade oscillations have been averaged out [*Dickman*, 1977]. TPW denotes a real displacement of the axis of rotation with respect to the geography and it is interesting to note that the TPW velocity is comparable with the velocities of the plates. Because of this coincidence of plate and TPW velocities, it has been argued in the past that polar wander is not a real motion of the axis of rotation but rather an artifact of the motion of the plates (apparent polar wander). It is only after the discovery of the relative fixity of the hot spot reference frame (hot spots move with respect to each other with typical velocities of about 1 cm yr^{-1}, while plates move with respect to each other with typical velocities of about 10 cm yr^{-1}) that a general consensus on the feasibility of TPW for a deforming planet like the Earth has been reached. TPW is a direct consequence of slow relaxation within the mantle following the readjustment of internal and surface loads. It is possible to establish (true) polar wander on a million year timescale from paleomagnetic data and the accurate determination of today's position of the rotation pole by means of modern space techniques, with respect to this relatively fixed hot spot reference frame. Although the true nature of

hot spots is still a matter of debate, one could associate them with more or less stationary mantle convection patterns. This would imply that whenever a large change of the global convection pattern emerges, being accompanied by a large reorganization of the plates, then the concept of true polar wander becomes meaningless as the hot spot reference frame is destroyed or reorganized. This limits the concept of TPW to periods of about 100 Myr, and one should be careful not to misinterpret a redistribution of hot spots during plate reorganization periods as a "catastrophic turnover" of the rotation axis. Apart from this, there is evidence of TPW on both timescales of millions of years [*Besse and Courtillot*, 1991] and thousands of years [*Dickman*, 1977]. On the million year timescale, subduction [e.g., *Ricard et al.*, 1992] and mantle convection [e.g., *Steinberger and O'Connell*, 1997] are considered to be the major contributors to TPW, while on the thousand year timescale the redistribution of surface loads due to the growing and melting of huge ice sheets is considered to be one of main forcing mechanisms for TPW. The major evidence in support of this interpretation for present-day polar wander stands on the direction of the motion shown in Figure 1, which is the direction that one gets when the excitation functions of the two largest Pleistocene ice sheets, the Laurentian and Fennoscandian, are summed vectorially in the Liouville equations. However, it should be kept in mind that this fact is not the same as a proof. It has also been suggested that tectonic processes like subduction [e.g., *Ricard et al.*, 1992], fast subsidence of ocean basins and detachment of subducting slabs [*Vermeersen and Vlaar*, 1993], mountain building [*Vermeersen et al.*, 1994], and mantle convection [*Steinberger and O'Connell*, 1997] might contribute to the present-day secular drift of the rotation axis. However, in this paper we will assume that only Pleistocene deglaciation drives the present-day TPW and changes in J_2, thereby also neglecting a possible influence of contemporary glacier and small ice sheet glaciations and deglaciations [e.g., *Sabadini et al.*, 1988; *James and Ivins*, 1997]. This neglect is one of the major uncertainties in deriving information on mantle viscosity from combined models on TPW and changes in J_2. *Steinberger and O'Connell* [1997] derive from their mantle heterogeneities advection model a contribution of 40% to the observed secular TPW rate. Contemporary forcings might induce TPW rates comparable to the secular TPW velocity: some of the models of *Vermeersen et al.* [1994] on (geoid-constrained) neotectonics of the Himalayas and Tibetan Plateau and of *James and Ivins* [1997] on mass changes of the Greenland ice sheet induce TPW velocity rates which are comparable to the observed present-day TPW rate. Taken together, all these geophysical forcings (mantle convection, tectonics, present-day ice and water redistributions, etc.), with their associated uncertainties, make it very difficult to extract unique information about the viscosity of the Earth's mantle from TPW simulations.
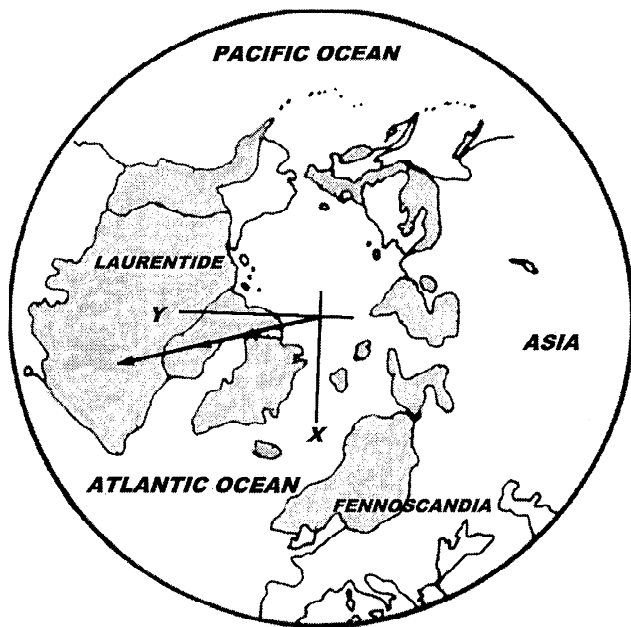
Figure 1. Cartoon showing the Pleistocene ice sheets and the direction of the present-day secular wander of the rotation axis. Polar motion is given in the conventional international origin (CIO) coordinates (x axis through Greenwich), on the basis of the reduction of the International Latitude Service data as described by *Dickman* [1977].

Other uncertainties that accompany deriving radial viscosity profiles from rotational studies are the neglect of lateral viscosity variations and uncertainties in the load history of the Pleistocene ice models. There are reasons, however, that these will affect the results to a lesser extent. Although pretty large lateral variations in viscosity are very likely to be present in the upper mantle, their influence on second-degree harmonics is found to be small [*D'Agostino et al.*, 1997]. For low-degree phenomena like Earth rotation and global geoid changes we thus expect that volume averaging over lateral viscosity variations in the upper mantle and using this value in our models will give about the same results as when models are used in which these lateral viscosity variations are retained. To put this in another way, it might be very difficult to obtain information on lateral viscosity variations from (degree 2) rotational data, just as it is also difficult to obtain detailed information on the radial viscosity profile for a large number of layers from studying harmonic degree 2 phenomena only. Indeed, *Vermeersen and Sabadini* [1997] have found that for harmonic degree 2, saturated continuum limits are reached for the Love numbers for models with a small amount of layers largely independent of the form of the radial viscosity profile. Considering this, and considering the uncertainties with respect to the forcing mechanisms, we have decided to take only two viscosity layers in our models, whereas the elastic parameters and density that we use (PREM) are more fine graded.

Also, uncertainties in the ice load history are expected to have less influence than uncertainties in the forcing mechanisms. From earlier studies [e.g., *Wu and Peltier*, 1984], it is known that the final ice age has the most impact on the present-day rotational changes, thereby diminishing the influence of uncertainties in the history of former Pleistocene ice cycles.

2. Theory

The theory that is used to study changes in the second-degree harmonic of the geoid J_2 and polar wander can be found in a number of publications over the past 15 years [e.g., *Nakiboglu and Lambeck*, 1980; *Sabadini and Peltier*, 1981; *Sabadini et al.*, 1982, 1984; *Wu and Peltier*, 1984; *Peltier*, 1985; *Spada et al.*, 1992; *Ricard et al.*, 1992, 1993; *Mitrovica and Peltier*, 1993; *Vermeersen et al.*, 1994, 1996b; *Peltier and Jiang*, 1996]. The models in all these references employ a viscoelastic Maxwell rheology for a spherical Earth model (that is, normal mode theory is first applied to a nonrotating spherical Earth model after which the required rotating ellipsoidal Earth model is obtained by applying the centrifugal potential). Differences in the models of the above references exist in, for example, the number of layers that the Earth model has, the way in which the differential equations are solved (analytically or numerically), whether the Lamé parameter λ is taken to be finite or infinite (compressible or incompressible), and whether the models allow only for surface loads or also for internal mantle loads.

The normal mode method that we use is described extensively in *Vermeersen et al.* [1996a] and *Vermeersen and Sabadini* [1997]. In general, for each layer of the model the differential equations for quasi-static viscoelastic deformation can be solved analytically in the Laplace-transformed domain. These general solutions (that is, solutions with undetermined integration constants) can be composed in the form of fundamental matrices and, consequently, used in a standard propagator matrix method. Inverse Laplace transformation results in a (known) number of relaxation times, each corresponding to a relaxation mode. The number of relaxation modes is a function of the Earth model. Depending on the kind of forcing, the strengths of the modes can be determined. These are then used to assemble the various signatures (stress, deformation, gravity, geoid changes, polar wander, etc.).

The theories developed by *Sabadini et al.* [1982] and by *Wu and Peltier* [1984] have been shown to be equivalent by *Sabadini et al.* [1984] and *Vermeersen and Sabadini* [1996]. Specifically, *Sabadini et al.* [1984] have shown that the secular polar wander terms (see equation (3)) are the same, while *Vermeersen and Sabadini* [1996] have demonstrated that when the Chandler wobble is filtered from the model of *Sabadini et al.* [1982], then to a high approximation the same polar wander curves are obtained compared to those found with the model

of *Wu and Peltier* [1984] for all timescales. A detailed proof of the equivalence of the theories of *Sabadini et al.* [1982] and *Wu and Peltier* [1984] with respect to the treatment of the Chandler wobble is given by *Mitrovica and Milne* [1997].

In *Spada et al.* [1992] the analytical theory is developed for polar wander and $\dot{J}_2$ models for Earth stratifications with five layers at most. *Vermeersen et al.* [1996a] and *Vermeersen and Sabadini* [1997] have developed the analytical theory for the relaxation of an Earth model consisting of a general amount of layers. In this section we concentrate on those aspects that are specifically associated with studying rotational changes by means of analytical models in which the Earth is radially stratified with a general amount of layers.

The formulas for polar wander and $\dot{J}_2$ can be written in the Laplace domain in a compact form. The time-derivative of the second-degree harmonic of the geoid $\dot{J}_2$ can be written in the Laplace domain, with s denoting the Laplace-transformed variable and a tilde denoting Laplace-transformed variables, as [e.g., *Sabadini et al.*, 1988]

$$\dot{\tilde{J}}_2(s) = -\frac{3}{2M_E a^2}\left(1 + k_e^L + \sum_{j=1}^{M}\frac{k_j^L}{s - s_j}\right)I_{33}^R \times s\tilde{f}(s) \quad (1)$$

where $\tilde{f}(s)$ is the Laplace-transformed loading history in (1). M_E is the mass of the Earth with radius a, k_e^L is the elastic load Love number, and the terms k_j^L are the load Love numbers of the M modes j with (negative) inverse relaxation times s_j. Note that the load Love numbers k_j^L have the same dimension as the inverse relaxation times s_j (for some of the readers it might look awkward that we define here a "Love number" which has a time dimension; although originally the terms "Love numbers" and "Love-Shida numbers" have been used in a rather strict sense, with the development of time-dependent relaxation modeling it has become common practice to extend their use, apart from the more classical "elastic" and "fluid" Love numbers, to the transient parts in the way described here). The relaxation times and Love numbers of the various modes are determined by the analytical models of *Vermeersen et al.* [1996a] and *Vermeersen and Sabadini* [1997].

For the case of a circular disk load with mass M_I and radius α at glacial maximum, with its center at colatitude θ and eastern longitude ϕ, and with the melted ice redistributed over the oceans with a realistic ocean function, the rigid earth inertia perturbation I_{33}^R is given by [*Wu and Peltier*, 1984, equation (28)]

$$I_{33}^R = M_I a^2\left[\frac{2}{15}\frac{a_{20}}{a_{00}} - \frac{cos\ \alpha(1 + cos\ \alpha)}{3}P_2(cos\ \theta)\right]. \quad (2)$$

The quotient a_{20}/a_{00} is determined from the expansion of the ocean function in spherical harmonics [e.g., *Lambeck*, 1980]. P_2 is the second-degree Legendre polyno-

mial. In our models the ice and water distribution is redistributed eustatically over the oceans. *Mitrovica and Peltier* [1993] report that for J_2, differences of 10-15% can be expected with those models which include a gravitationally self-consistent redistribution of the meltwater.

In complex notation, with $i = \sqrt{-1}$, the polar wander m derived from the linearized Liouville equation [e.g., *Munk and MacDonald*, 1960] is given in the Laplace domain by [e.g., *Spada et al.*, 1992, equations (10)-(12)]

$$\tilde{m}(s) = -i\sigma_r\frac{I_{13}^R + iI_{23}^R}{C - A}\left(\frac{A_0}{s} + \sum_{i=1}^{M}\frac{A_i}{s - a_j}\right)$$
$$\times\left(1 + k_e^L + \sum_{j=1}^{M}\frac{k_j^L}{s - s_j}\right)\tilde{f}(s) \quad (3)$$

where $\tilde{m}(s)$ is the Laplace-transformed complex-valued polar wander, defined in such a way that the real-valued component gives the polar wander in the direction of the Greenwich Meridian and the imaginary-valued component gives the polar wander in the direction 90o to the east. The σ_r is the Chandler wobble frequency for a rigid Earth. C and A are the principal moments of inertia. The rigid Earth perturbations in the product-of-inertia components I_{13}^R and I_{23}^R are for the same load as that used in (2) and are given by [*Wu and Peltier*, 1984, equation (28)]

$$I_{13}^R = -M_I a^2\left[\frac{1}{6}cos\ \alpha(1 + cos\ \alpha)P_{21}(cos\ \theta)cos\ \phi\right.$$
$$\left. -\frac{1}{5}\frac{a_{21}}{a_{00}}\right], \quad (4)$$

$$I_{23}^R = -M_I a^2\left[\frac{1}{6}cos\ \alpha(1 + cos\ \alpha)P_{21}(cos\ \theta)sin\ \phi\right.$$
$$\left. -\frac{1}{5}\frac{b_{21}}{a_{00}}\right]. \quad (5)$$

The quotients a_{21}/a_{00} and b_{21}/a_{00} can again be found from the spherical harmonic expansion of the ocean function [e.g., *Lambeck*, 1980]. P_{21} is the second-degree, first-order Legendre polynomial given by $P_{21}(cos\ \theta) = 3\ cos\ \theta\ sin\ \theta$. Note that this is the negative of what is presented in *Wu and Peltier* [1984], resulting in the extra minus sign of (4) and (5) with respect to the corresponding terms in *Wu and Peltier*'s [1984] (28) [see also *Peltier and Jiang*, 1996]. The (negative) inverse relaxation times a_i and their associated complex-valued residues A_i for the M modes i are found by considering the relaxation due to a centrifugal forcing. A_0 is dubbed the secular term [*Munk and MacDonald*, 1960]. Equation (3) can be further simplified to [e.g., *Vermeersen et al.*, 1994]

$$\tilde{m}(s) = -i\sigma_r\frac{I_{13}^R + iI_{23}^R}{C - A} \times \left(\frac{A_0^*}{s} + \sum_{i=1}^{M}\frac{\beta_i}{s - s_i}\right.$$
$$\left. +\sum_{i=1}^{M}\frac{\gamma_i}{s - a_i}\right)\tilde{f}(s) \quad (6)$$

in which

$$\beta_i = A_0 \frac{k_i^L}{s_i} + \sum_{j=1}^{M} \frac{A_j k_i^L}{s_i - a_j} \qquad (7)$$

$$\gamma_i = A_0(1 + k_e^L) - \sum_{j=1}^{M} \frac{A_i k_j^L}{s_j - a_i} \qquad (8)$$

$$A_0^* = A_0(1 + k_f^L) \qquad (9)$$

in which the fluid limit ($s = 0$) of the load Love number is given by

$$k_f^L = k_e^L - \sum_{i=1}^{M} \frac{k_i^L}{s_i} \qquad (10)$$

It can be proven analytically that the coefficients β_i are equal to zero [*Bills and James*, 1997; *Vermeersen*, 1993, equations (4.40) and (4.47)].

For the loading history $f(t)$ we took the loading history of ICE-3G of *Tushingham and Peltier* [1991] and extended this ice model to eight complete glacial cycles (Figure 2). ICE-3G consists of a total of 808 circular disk loads, representing the Laurentide ice sheet, the Fennoscandian ice sheet, the northern part of Russia, Antarctica, and the southwest of South America. For all these disks, ICE-3G gives the ice decay of the last Pleistocene cycle by a set of decrements, starting at 18 kyrs before present and ending at 5 kyrs before present. The Antarctic ice sheet starts to melt at a later stage than the ice sheets of the northern hemisphere. The total ice mass of all the disks is plotted as a function of time in Figure 3 (there are some negligibly small changes from 5 to 3 kyrs before present; from 3 kyrs to present the ice masses of all disks remain constant). Our eight complete glacial cycles consist of seven glacial sawtooth precycles, while the eighth cycle consists of a linear glaciation phase which ends at 18 kyrs before present followed by ICE-3G. Each cycle is connected to its previous and following ones. Each of the seven pre-

cycles consists of a 90 kyrs linear growth phase and a 10 kyrs linear decay phase. The minimum amount of ice is the same as in ICE-3G at present, while the maximum amount of ice is the same as in ICE-3G at 18 kyrs before present. Both the polar wander rates and the $\dot{J}_2$ rates are determined at present.

For this temporal history the Laplace-transformed function $\tilde{f}(s)$ can be easily determined and substituted in the multidisk equivalents of the above formulations. The temporal history is simple enough, consisting of a combination of Heaviside functions and linear functions, so that performing the inverse transformations of (1) and (6) can be done analytically.

The TPW models can be relatively easily implemented in computer codes when all inverse relaxation times s_i and a_i are detected by a root-finding procedure. This is certainly the case with models which only have a limited amount of layers, such as the five layer models used in *Spada et al.* [1992]. Problems arise when not all roots are found, as is rather the rule than the exception in models with a large amount of layers. In models where only load relaxation is important, as for $\dot{J}_2$, it does not matter when modes are not taken into account (or which remain undetected) that have a far too low strength to be of any importance. This is the case, for instance, for those long-term buoyancy modes which are triggered by small density contrasts between two layers [*Han and Wahr*, 1995; *Vermeersen and Sabadini*, 1997]. However, for polar wander it is absolutely necessary that when the mode i associated with the inverse relaxation time s_i is taken into account, its rotational counterpart a_i is also taken into account.

If the root finder for the modes associated with the inverse relaxation times a_i is not able to detect all a_i for the corresponding load-relaxation counterparts s_i in our codes, then we apply the following procedure. First, the parameters x_i, defined by [*Vermeersen and Sabadini*, 1996]
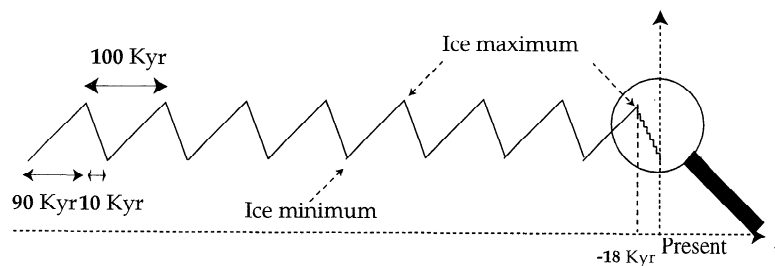
$$x_i = \frac{\sigma_r k_i^T}{k_f^T s_i} \qquad (11)$$

Figure 2. Pleistocene glaciation and deglaciation history as used in the models. The history contains seven glacial ramp-shaped cycles followed by a linear ice accumulation period and a deglaciation period consisting of a set of discrete unloading steps (after ICE-3G [*Tushingham and Peltier*, 1991]). Each cycle has a 90 kyr glaciation period. The seven glacial precycles have deglaciation periods of 10 kyr. The final glacial cycle, which starts at 18 kyr before present, has a 13 kyr deglaciation period of Heaviside loadings. The ice masses are assumed to remain constant after 5 kyr before present. The maximum amount of ice that is accumulated at the end of a glaciation period is the same as ICE-3G gives at 18 kyr before present. The minimum amount of ice at the end of a deglaciation period is the same as ICE-3G gives at 5 kyr before present.
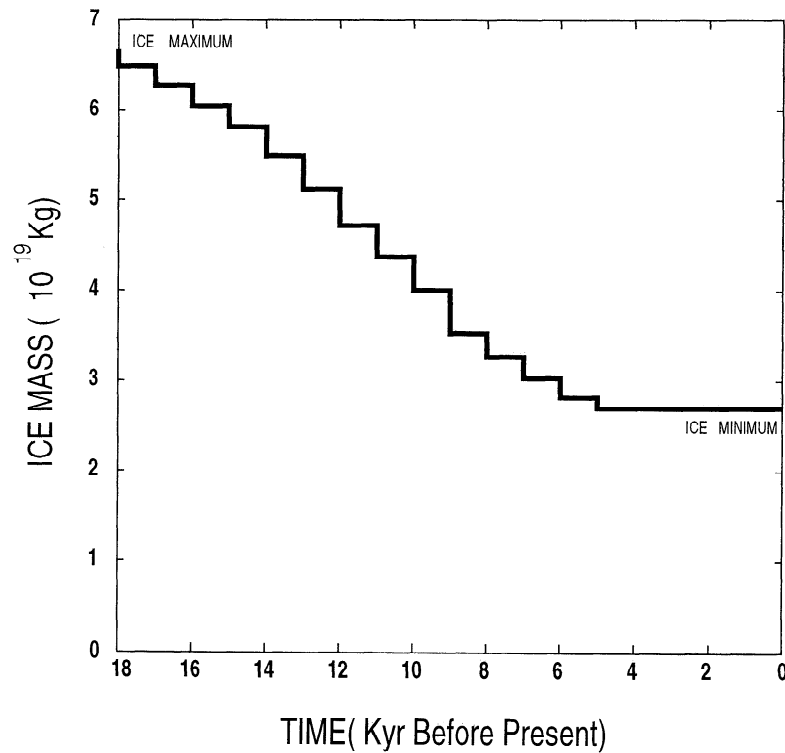
Figure 3. Enlargement of the final deglaciation phase of Figure 2. The discrete time steps of the ICE-3G model are shown. The ice mass on the vertical axis represents the ice of all sheets.
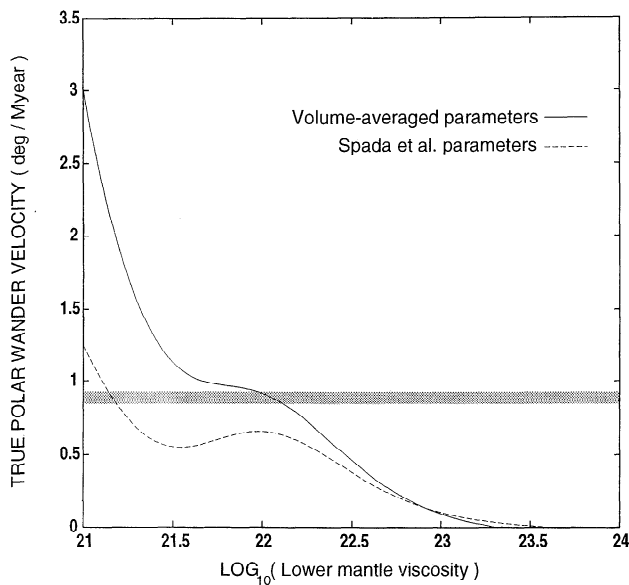

Figure 4. The present-day true polar wander velocity as a function of the lower mantle viscosity for two five-layer Earth models. For this figure the ice load consisted of the Fennoscandian, Laurentian, and Antarctic ice sheets modeled as homogeneous disks. The value of the viscosity of the upper mantle is 10^{21} Pa s. The solid curve depicts the solution by the volume-averaged Earth model of Table 1, and the dashed curve depicts the solution from the fixed boundary contrast Earth model of Table 2 as used in *Spada et al.* [1992]. The lightly hatched area depicts the observed present-day secular drift ranging between the error bars as given by *Dickman* [1977]. The darkly hatched area depicts the observed present-day secular drift ranging between the error bars as given by *McCarthy and Luzum* [1996].

in which k_i^T are the tidal-effective Love numbers of the modes i and k_f^T is the fluid tidal-effective Love number, are determined. These parameters x_i, which can be thought of as renormalized strengths of the load relaxation modes i, give also a good indication of the strength of the corresponding rotational modes [*Vermeersen and Sabadini*, 1996]. When not all rotational counterparts for the load relaxation modes are detected by the root-finding procedure, then those modes which have the lowest values for x_i are skipped until all rotational counterparts are detected. In practice, this procedure causes only a few of the modes to be deleted for models carrying more than 30 layers. Those modes that are deleted commonly have orders of magnitude smaller strengths than the five or six most important modes. Inaccuracies in polar wander rates thus do not arise from this deletion procedure but from the contributions from load-relaxation roots which remain undetected by the root-finding procedure. For the root-finding procedure we have used, we refer to *Vermeersen and Sabadini* [1997].

3. 10^{21} Pa s Upper Mantle Viscosity

The first TPW results, for a viscosity of 10^{21} Pa s in the upper mantle and varying lower mantle viscosity, are portrayed in Figure 4. In this figure, only the Laurentide, Fennoscandian, and Antarctic ice sheets are taken into account as disks, in agreement with the previous analyses by *Yuen et al.* [1986] and *Spada et al.* [1992]. Figure 4 shows, within the scheme of a five-layer model consisting of the lithosphere, three layers in the mantle and a core, the effects of constraining the aver-

age values of the density and rigidity in each layer on the basis of PREM (solid curve) or, alternatively, the effects of constraining the density and rigidity contrasts at the 420 and 670 km discontinuities in agreement with PREM (dashed curve). The latter procedure was used in the past in TPW models based on analytical schemes [*Sabadini et al.*, 1982; *Yuen et al.*, 1986; *Spada et al.*, 1992]. The values used in our five-layer models can be found in Table 1 for the volume-averaged model and in Table 2 for the fixed boundary contrast model. In the first case the contrasts at the interfaces are overestimated, while in the second case the densities of the layers do not reproduce the average values of PREM. The two schemes predict quite different TPW signals, although the major characteristics of the two curves are the same: a general decay from high TPW value for an isoviscous mantle, the vanishing of the signal for a lower mantle viscosity of 10^{23} Pa s, and a nonmonotonic behavior from 3×10^{21} to 10^{22} Pa s. The fixed boundary contrast model (dashed curve) portrays a well-developed local maximum at 10^{22} Pa s. In particular, the dashed curve crosses the observational datum of *McCarthy and Luzum* [1996] for a lower mantle viscosity of 1.5×10^{21} Pa s. On the basis of this result an almost homogeneous mantle was deduced from previous TPW and $\dot{J}_2$ studies [*Sabadini et al.*, 1982; *Yuen et al.*, 1986; *Spada et al.*, 1992]. The extra buoyancy of the model with volume-averaged densities is responsible for an increase in the TPW signal in the whole range of lower mantle viscosities, which has the major effect of displacing the crossing of the TPW curve with the observed values to higher viscosities. As we will see in the following, this result has a major impact on the interpretation of the viscosity profile of the mantle based on TPW analysis.

Figure 5 shows the effects of distributing the density contrasts of the mantle in a large number of layers. PREM contains 56 layers in the lithosphere and mantle. The 31-layer model of Table 3 is deduced from PREM in such a way that the layers get a progressively larger thickness from the Earth's surface to the core, in agreement with the findings of *Vermeersen and Sabadini* [1997]. With respect to the simpler five-layer model with volume-averaged densities the buoyancy is now smoothly distributed over the mantle instead of being concentrated at the four major boundaries. Lay-

ering has, in fact, a major effect because it modifies the TPW curve in the proximity of the inflection of the curve at a lower mantle viscosity of 10^{22} Pa s, where crossing with the observations occurs. While for lower mantle viscosities ranging from 10^{21} to 3×10^{21} Pa s, density stratification has negligible effects, PREM predicts a quite different behavior with respect to the simpler five-layer model for viscosities higher than 3×10^{21} Pa s. In fact, the TPW signal increases in the proximity of the observational data, causing a multiplicity of lower mantle viscosity solutions. These results indicate a trade-off between density and viscosity stratification in the mantle. Another remarkable result of this figure is that differences between the curves corresponding to 31 and 56 layers are negligible, indicating that as far as rotational calculations are concerned, the continuous behavior in the sense discussed by *Vermeersen and Sabadini* [1997] has already been reached with 31-layer models. Increasing the number of layers does not provide any further information on TPW.

It is interesting to compare the sensitivity of TPW with respect to density stratification with that portrayed by $\dot{J}_2$. In Figure 6, $\dot{J}_2$ is shown for a 5-layer and 31-layer model with a fixed upper mantle viscosity of 10^{21} Pa s and varying lower mantle viscosity. Density stratification has no effects on $\dot{J}_2$ between a 5-layer model and PREM once volume-averaged parameters are used. This different behavior with respect to TPW is not surprising since TPW solutions have the extra viscoelastic readjustment of the equatorial bulge above the load readjustment, which is the only one present in $\dot{J}_2$.

4. Variations in Depth of the Two-Layer Mantle Viscosity Profile

In this section we consider the possibility that the boundary where the viscosity contrast occurs does not coincide with the seismologically inferred base of the upper mantle. Two depths are considered, 971 and 1471 km, so both are deeper than the 670 km one shown for comparison. The 1471 km depth is close to the depth of 1400 km considered in the relative sealevel (RSL) analysis by *Mitrovica* [1996] and the TPW and $\dot{J}_2$ studies by *Peltier and Jiang* [1996], while 971 km is an intermediate value.

Table 1. Parameters for the Five-Layer Volume-Averaged Earth Model

Layer	R, km	ρ, kg m^{-3}	μ, N m^{-2}	Stratification
1	6371 − 6250	3184.3	6.0243×10^{10}	lithosphere
2	6250 − 5951	3434.2	7.2666×10^{10}	shallow upper mantle
3	5951 − 5701	3856.7	1.0639×10^{11}	transition zone
4	5701 − 3480	4877.5	2.1944×10^{11}	lower mantle
5	3480 − 0	10925	0	inviscid fluid core

R is the distance with respect to the center of the Earth; ρ is the density of the layer; and μ is the rigidity.

Table 2. Parameters for the Five-Layer Fixed-Boundary Contrast Earth Model

Layer	R, km	ρ, kg m^{-3}	μ, N m^{-2}	Stratification
1	6371 − 6271	4120	7.28×10^{10}	lithosphere
2	6271 − 5951	4120	9.54×10^{10}	shallow upper mantle
3	5951 − 5701	4220	1.10×10^{11}	transition zone
4	5701 − 3480	4508	1.99×10^{11}	lower mantle
5	3480 − 0	10925	0	inviscid fluid core

R is the distance with respect to the center of the Earth; ρ is the density of the layer; and μ is the rigidity.

For the upper layer viscosity fixed at 10^{21} Pa s, Figure 7 portrays the TPW curves for the three different depths as a function of the lower layer viscosity. Increasing the viscosity in the lower layer has the effect of reducing the TPW from about $3°$ Myr^{-1} for a viscosity of 10^{21} Pa s to zero. Although the shape of the curves is the same for the three different depths, the deepening of the viscosity contrast has the major effect of diminishing the local maximum at 10^{22} Pa s. For 1471 km this local maximum disappears and is barely visible for 971 km. The modification in the shape of the curves has the important consequence of reducing the ambiguity in the inference of the lowermost viscosity from the admissible range of $2.8 \times 10^{21} - 1.5 \times 10^{22}$ Pa s for 670 km to the narrower range of $3 - 5 \times 10^{21}$ Pa s for 1471 km when *Dickman's* [1977] data are considered. The most recent TPW data by *McCarthy and*

Luzum [1996] require a value of 4×10^{21} Pa s, being intermediate between the two previous estimates. Notice that, irrespective of the depth of the boundary, the same value of TPW is retrieved when the lowermost viscosity equals the viscosity of the upper layer, as expected. The results shown in Figure 7 are in distinct contrast with those portrayed by *Peltier and Jiang* [1996] in their Figures 7c and 9a. The major difference with respect to our results stands on the drastic modification of the TPW curves when the viscosity contrast is moved from 670 to 1470 km. At first glance the TPW curve by *Peltier and Jiang* [1996; Figure 9a], corresponding to the case of 1400 km, is displaced to the right with respect to their Figure 7c. This displacement is toward higher viscosities, which seems to prevent the same TPW from being reproduced when both the upper and lower layers have the same viscosity of 10^{21} Pa s. This equality should be the case when the TPW curve in their Figure 9a is continued to 10^{21} Pa s. TPW for this viscosity value is not shown in their Figure 9a, but because of the behavior of the curve that shows a monotonic increase when the lower mantle viscosity is varied to lower values, it is difficult to imagine that the value of $1.3°$ Myr^{-1} of Figure 7c of *Peltier and Jiang* [1996], corresponding to 10^{21} Pa s, could be reproduced unless a maximum is located somewhere between 10^{21} and 10^{22} Pa s. Another major difference in comparison to our results stands on the vanishing of TPW in Figure 7c of *Peltier and Jiang* [1996] for a depth of the boundary at 670 km and a lower mantle viscosity of about 10^{22} Pa s. We obtain, on the contrary, a local maximum of about $0.9°$ Myr^{-1}. It should be emphasized that a nonmonotonic decrease in TPW, as shown by *Yuen and Sabadini* [1984] and *Spada et al.* [1992], consistent with the results shown in the present paper with a local maximum in proximity of 10^{22} Pa s, is also obtained in a recent analysis by *Milne and Mitrovica* [1996] based on compressible models. Recently, both *Mitrovica and Forte* [1997] and *Mitrovica et al.* [1997] have pointed out that the results obtained in *Peltier and Jiang* [1996] must be in error.

Figure 8 deals with a similar analysis for $\dot{J}_2$. The most apparent effects of the lowering of the viscosity contrast are the disappearance of the high-viscosity solution branch of 2×10^{23} Pa s for 1471 km in the right
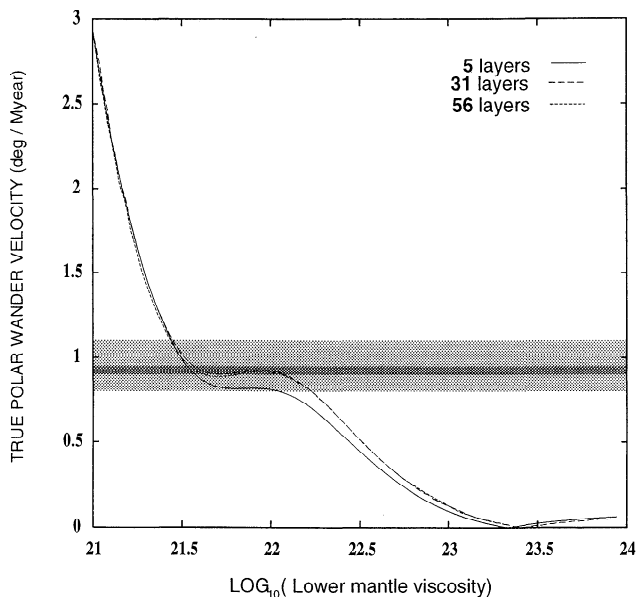

Figure 5. The present-day true polar wander velocity as a function of the viscosity of the lower mantle for a volume-averaged Earth model. The upper mantle has a viscosity of 10^{21} Pa s. The number of layers for the three curves is indicated in the top right corner. The hatching has the same meaning as in Figure 4.

Table 3. Parameters for the Standard 31-Layer Volume-Averaged Earth Model Derived From the Preliminary Reference Earth Model (PREM)

Layer	R, km	ρ, kg m^{-3}	μ, N m^{-2}	Stratification
1	6371.0 − 6368.0	1020	2.66×10^{10}	lithosphere
2	6368.0 − 6356.0	2600	2.66×10^{10}	lithosphere
3	6356.0 − 6346.6	2900	4.41×10^{10}	lithosphere
4	6346.6 − 6331.0	3372	6.81×10^{10}	lithosphere
5	6331.0 − 6311.0	3372	6.78×10^{10}	lithosphere
6	6311.0 − 6291.0	3372	6.75×10^{10}	lithosphere
7	6291.0 − 6251.0	3372	6.71×10^{10}	lithosphere
8	6251.0 − 6221.0	3372	6.67×10^{10}	shallow upper mantle
9	6221.0 − 6186.0	3372	6.63×10^{10}	shallow upper mantle
10	6186.0 − 6151.0	3372	6.58×10^{10}	shallow upper mantle
11	6151.0 − 6106.0	3449	7.48×10^{10}	shallow upper mantle
12	6106.0 − 6061.0	3476	7.64×10^{10}	shallow upper mantle
13	6061.0 − 6016.0	3503	7.81×10^{10}	shallow upper mantle
14	6016.0 − 5971.0	3529	7.97×10^{10}	shallow upper mantle
15	5971.0 − 5921.0	3755	9.39×10^{10}	transition zone
16	5921.0 − 5871.0	3819	1.01×10^{11}	transition zone
17	5871.0 − 5821.0	3882	1.09×10^{11}	transition zone
18	5821.0 − 5771.0	3945	1.17×10^{11}	transition zone
19	5771.0 − 5736.0	3980	1.21×10^{11}	transition zone
20	5736.0 − 5701.0	3988	1.23×10^{11}	transition zone
21	5701.0 − 5650.0	4397	1.59×10^{11}	lower mantle
22	5650.0 − 5600.0	4423	1.68×10^{11}	lower mantle
23	5600.0 − 5400.0	4501	1.78×10^{11}	lower mantle
24	5400.0 − 5200.0	4620	1.91×10^{11}	lower mantle
25	5200.0 − 4900.0	4759	2.06×10^{11}	lower mantle
26	4900.0 − 4600.0	4921	2.24×10^{11}	lower mantle
27	4600.0 − 4300.0	5078	2.41×10^{11}	lower mantle
28	4300.0 − 4000.0	5205	2.58×10^{11}	lower mantle
29	4000.0 − 3700.0	5379	2.74×10^{11}	lower mantle
30	3700.0 − 3480.0	5509	2.89×10^{11}	lower mantle
31	3480.0 − 0	10932	0	inviscid fluid core

R is the distance with respect to the center of the Earth; ρ is the density of the layer; and μ is the rigidity.

portion of the figure and the smooth increase, from $1.5-2.8 \times 10^{21}$ to $2.5-5 \times 10^{21}$ Pa s, of the low-viscosity branch. The increase in the $\dot{J_2}$ signal for the lowermost mantle viscosities higher than 3×10^{21} Pa s when the viscosity contrast is located deeper than 670 km agrees with the results of *Mitrovica and Peltier* [1993].

This behavior in the $\dot{J_2}$ curve has the important implication of allowing for a single solution in the lowermost viscosity and, when comparison is made with the TPW curve for 1471 km of Figure 7, allowing for the simultaneous fit of the TPW and $\dot{J_2}$ data with a viscosity in the lower layer of $3-5 \times 10^{21}$ Pa s when the TPW data by *Dickman* [1977] are considered and 4×10^{21} Pa s with the latest TPW data [*McCarthy and Luzum*, 1996]. For 670 km it is not possible to obtain a simultaneous fit of both TPW and $\dot{J_2}$ for any value of the lower mantle viscosity when the new TPW data are considered. With *Dickman*'s [1977] TPW data the two viscosity solutions barely overlap at 2.5×10^{21} Pa s, degrading the simultaneous TPW and $\dot{J_2}$ fit for the depth of the viscosity

contrast at 670 km with respect to 1471 km. If the same comparison between our $\dot{J_2}$ analysis and Figure 9b of *Peltier and Jiang* [1996] is performed, the conclusions are similar to the ones of the previous figure. In *Peltier and Jiang* [1996, Figure 9b] the $\dot{J_2}$ curve appears to be displaced to the right with respect to their Figure 8b, again prohibiting the same $\dot{J_2}$ value from being reached when the mantle viscosity is uniformly fixed at 10^{21} Pa s in both layers, thus reproducing the same inconsistency addressed above. As for the case of TPW, *Peltier and Jiang* [1996] thus predict a higher viscosity in the lowermost layer of 10^{22} Pa s. The different findings of the present analysis with respect to *Peltier and Jiang* [1996] cannot be due to different formulations, as shown in *Vermeersen and Sabadini* [1996] where the equivalence of the two procedures in solving the rotational Liouville equations was demonstrated. Neither are (small) differences in the ice models, as low-degree phenomena as TPW and $\dot{J_2}$ are relatively insensitive to this (high harmonic degrees are, on the other hand).
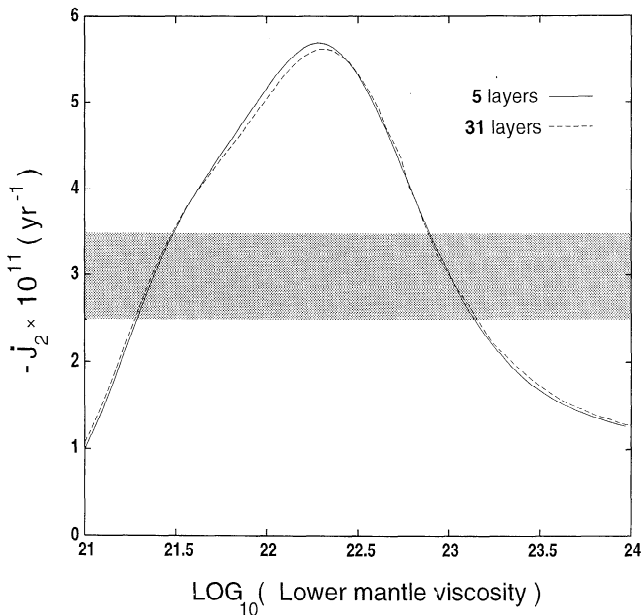
Figure 6. The secular variation in the present-day $\dot{J}_2$ as a function of the value of the viscosity of the lower mantle. The value of the viscosity of the upper mantle is fixed at 10^{21} Pa s. The two curves depict the results for a volume-averaged Earth model consisting of 5 layers and of 31 layers. The hatched area depicts the observed present-day $\dot{J}_2$ ranging between $(-2.5 \pm 0.7) \times 10^{-11}$ yr^{-1}, corresponding to the CGS-96 solution of the Italian Space Agency derived from LAGEOS I and LAGEOS II monthly estimates for the time interval 1985-1996 [*Devoti et al.,* 1997, lower bound], and for the estimate obtained by *Yoder et al.* [1983] (upper bound).

The correctness of our analytical normal mode and rotational formulation is guaranteed by benchmark calculations (T. S. James, personal communication, 1995; J. X. Mitrovica, personal communication, 1996; P. Johnston, personal communication, 1997).

The important conclusion that we can draw from the results of Figures 7 and 8 is that when self-consistent, viscoelastic, stratified Earth models are considered, a viscosity of 10^{21} Pa s cannot be limited to the seismically defined upper mantle but must be considered appropriate for a wider region of the mantle to depths of about 1400 km. It should be emphasized that this conclusion is strongly supported by the new TPW data [*McCarthy and Luzum,* 1996] that definitively rule out a viscosity of 10^{21} Pa s only for the upper mantle, while the TPW data by *Dickman* [1977] only show an indication in this sense because of the larger error bounds.

This finding is only apparently inconsistent with previous analyses based on incompressible rotational deformation models, as in *Sabadini et al.* [1982], *Yuen et al.* [1984], and *Spada et al.* [1992]. In these references a simultaneous fit of TPW and J_2 data was found from an assumed value for the viscosity of the upper mantle of 10^{21} Pa s and a moderate viscosity increase in the lower mantle by a factor of 2. However, these previous

results were derived from simplified four-layer or five-layer Earth models where the density contrasts at the internal boundaries were fixed according to PREM instead of the layers having volumetric density averages derived from PREM.

Our findings are in complete agreement with a similar analysis of RSL data by *Mitrovica* [1996], who, with a more rigorous scheme based on the resolving power of RSL kernels, has demonstrated that the value of 10^{21} Pa s is appropriate for a region of the mantle extending to greater depths than the upper mantle defined by seismology. The value of 10^{21} Pa s, first proposed by *Haskell* [1935], was, in fact, somehow arbitrarily limited to the upper mantle after modern seismology had located the boundary between the upper and lower mantles at 670 km, as pointed out by *Mitrovica* [1996].

5. Upper Mantle Viscosities Smaller Than 10^{21} Pa s

In the previous section we saw that within the framework of a multilayered, viscoelastic Earth model based on PREM a simultaneous fit to TPW and $\dot{J}_2$ data is not possible when the viscosity value of 10^{21} Pa s is limited to the upper mantle. In this section the depth of the viscosity contrast is fixed at 670 km and the upper mantle viscosity is modified in order to get a simultaneous fit with TPW and $\dot{J}_2$ data when the lower mantle viscosity is varied from 10^{21} to 10^{24} Pa s, as in the previous figures.
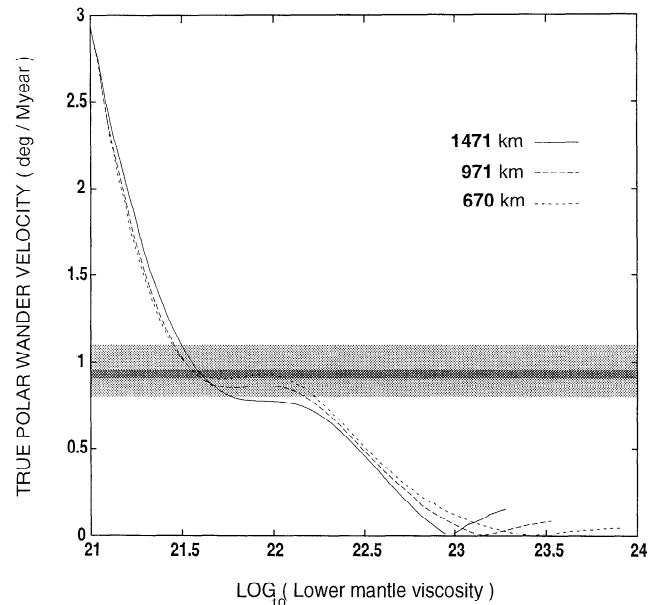

Figure 7. Effects of the depth of the viscosity contrast on the present-day true polar wander as a function of the value of the viscosity of the lower mantle. The standard 31-layer model of Table 3 is used as the Earth model. The three cases depict the results for the boundary between the upper and lower mantles (upper and lower mantle defined with respect to viscosity) at 1471, 971 and 670 km depth. The upper mantle has a viscosity of 10^{21} Pa s. The hatching has the same meaning as in Figure 4.
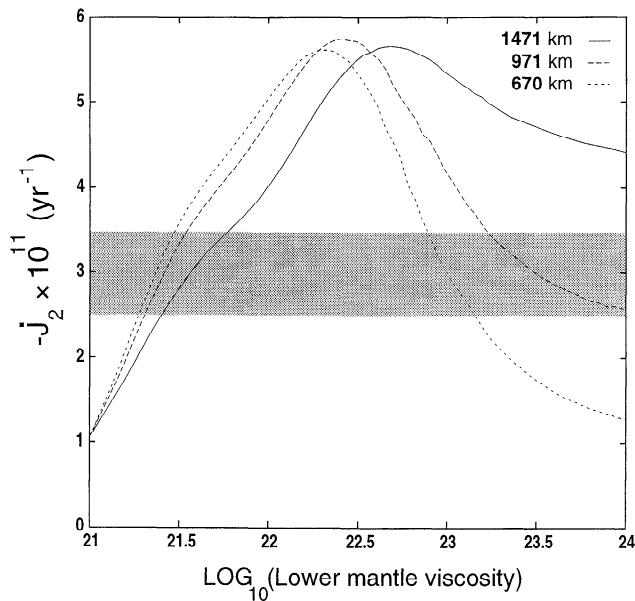
Figure 8. Effects of the depth of the viscosity contrast on the present-day secular variation in $\dot{J}_2$ as a function of the value of the viscosity of the lower mantle. The standard 31-layer model of Table 3 is used as the Earth model. The three cases depict the results for the boundary between the upper and lower mantles (upper and lower mantles are defined with respect to viscosity) at 1471, 971, and 670 km depth. The upper mantle has a viscosity of 10^{21} Pa s. The hatching has the same meaning as in Figure 6.

In Figure 9 the upper mantle viscosity is reduced from 10^{21} Pa s (dotted curve) to 10^{20} Pa s (solid curve); intermediate values are 5×10^{20} Pa s (short-dashed curve) and 2×10^{20} Pa s (long-dashed curve). The reduction in the upper mantle viscosity diminishes the TPW signal in the whole range of viscosities, but it should be noted that this occurs in a strongly nonlinear fashion. A factor of 2 reduction from 10^{21} Pa s to 5×10^{20} Pa s has minor effects, except for a small increase in the proximity of the local maximum at 10^{22} Pa s. A decrease of the upper mantle viscosity from 5×10^{20} Pa s to 2×10^{20} Pa s causes a further increase in proximity of the local maximum and a decrease in the range of lower mantle viscosities from 10^{21} to 4×10^{21} Pa s. This reduction in the signal is confirmed by the upper mantle viscosity of 10^{20} Pa s, which provides the smallest TPW values for lower mantle viscosities smaller than 10^{22} Pa s. Although in a nonlinear fashion, the reduction of the upper mantle viscosity has the effect of displacing the TPW curve to the left. Except for the lowest upper mantle viscosity of 10^{20} Pa s, which predicts a lower mantle of 2.5×10^{21} Pa s, the inference of the viscosity value of the lower mantle is not affected by a factor of 5 reduction from the reference value of 10^{21} Pa s. The reduction of the upper mantle viscosity has, on the other hand, the major effect of increasing the viscosity contrast at 670 km from 3 for the short-dashed curve

corresponding to 10^{21} Pa s, to 8 or 20 for the upper mantle viscosities of 5×10^{20} and 2×10^{20} Pa s, respectively.

In Figure 10, the same analysis is carried out for $\dot{J}_2$. The curves are the same as in Figure 9. As in the case of Figure 8, the major effects of the viscosity decrease are visible in the high-value region of the lower mantle viscosities for viscosities higher than 10^{23} Pa s. Major modifications with respect to the upper mantle viscosity of 10^{21} Pa s occur also in proximity of the maximum of the curves, and for lower mantle viscosities higher than 3×10^{21} Pa s.

The reduction of the peak value located at the lower mantle viscosity of 3×10^{22} Pa s and the increase in the signal for lower mantle viscosities larger than 10^{23} Pa s agree with the results obtained by *Mitrovica and Peltier* [1993]. The reduction of the upper mantle viscosity is responsible for an increase of the range of admissible lower mantle viscosities from $1.5 - 3 \times 10^{21}$ to $1.5 - 4 \times 10^{21}$ Pa s for an upper mantle viscosity of 10^{20} Pa s. With respect to the upper mantle value of 10^{21} Pa s, the $\dot{J}_2$ curves for reduced upper mantle viscosities are displaced to the right. This allows for a simultaneous fit with the TPW data of *McCarthy and Luzum* [1996] for a viscosity increase at 670 km that can be as high as factors of 20 and 30 for upper mantle viscosities of 2×10^{20} and 10^{20} Pa s, respectively. It should be noted
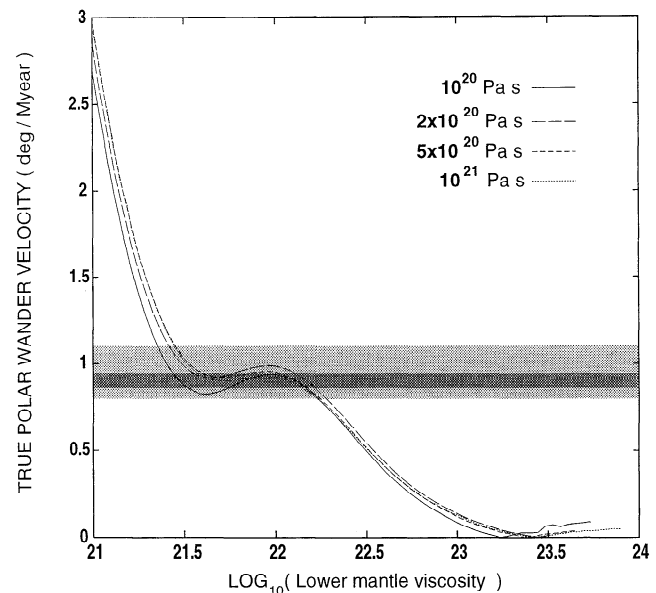

Figure 9. Effects of a lower value for the upper mantle viscosity on the present-day true polar wander as a function of the value of the viscosity of the lower mantle. The standard 31-layer model of Table 3 is used as the Earth model. The solid curve depicts the case of an upper mantle viscosity of 10^{20} Pa s. The dotted curve depicts the case of an upper mantle viscosity of 10^{21} Pa s. The two cases for the upper mantle viscosity in-between these two values are depicted by the short-dashed curve for the case of 5×10^{20} Pa s, and by the long-dashed curve for the case of 2×10^{20} Pa s. The hatching has the same meaning as in Figure 4.
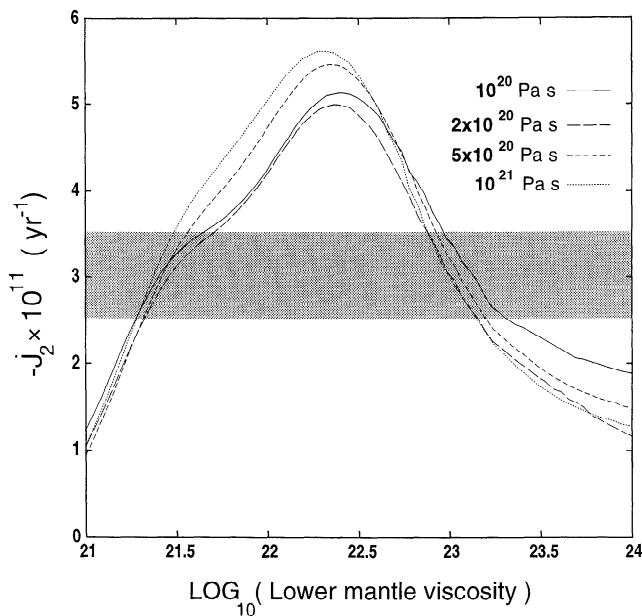
Figure 10. Effects of a lower value for the upper mantle viscosity on the the present-day secular variation in $\dot{J}_2$ as a function of the value of the viscosity of the lower mantle. The standard 31-layer model of Table 3 is used as the Earth model. The solid curve depicts the case of an upper mantle viscosity of 10^{20} Pa s. The dotted curve depicts the case of an upper mantle viscosity of 10^{21} Pa s. The two cases for the upper mantle viscosity in between these two values are depicted by the short-dashed curve for the case of 5×10^{20} Pa s and by the long-dashed curve for the case of 2×10^{20} Pa s. The hatching has the same meaning as in Figure 6.

that a simultaneous fit of TPW and $\dot{J}_2$ for an upper mantle viscosity of 5×10^{20} Pa s can only be obtained with the data of *Dickman* [1977], which have larger error bounds.

In comparison with the recent TPW data by *McCarthy and Luzum* [1996], those by *Dickman* [1977] are less discriminating in ruling out a viscosity value of 10^{21} Pa s above the 670 km discontinuity, although a clear tendency to prefer a lower value for the upper mantle viscosity is also shown by *Dickman*'s [1977] data by means of enlarging the interval of admissible viscosity solutions for the two data sets.

The upper and lower mantle viscosities of $1-5 \times 10^{20}$ and $2.5 - 4 \times 10^{21}$ Pa s inferred from the *McCarthy and Luzum* [1996] TPW data are consistent with the estimates made by *Lambeck et al.* [1990] of $3 - 5 \times 10^{20}$ and $2 - 7 \times 10^{21}$ Pa s for these parameters, although our results have the tendency to remain in the lower limit of *Lambeck et al.*'s [1990] predictions. This tendency is probably attributable to model differences with *Lambeck et al.*'s [1990] analysis, where attention is focused on a different postglacial rebound signal, such as sealevel in the far field, and compressible viscoelastic models with a lithospheric thickness smaller than ours. If we focus on the viscosity contrast at the bound-

ary between the upper and lower mantles, we obtain a complete agreement with the findings of *Lambeck et al.* [1990], whose preferred upper and lower mantle viscosity contrast ranges between a factor of 4 and 25.

Our upper and lower mantle viscosities are generally lower than the latest estimates of these parameters by *Lambeck et al.* [1996]. In their analysis of the glacial rebound of the British Isles the preferred upper mantle viscosity is 7×10^{20} Pa s, and the lower mantle viscosity is about 10^{22} Pa s for the case of the two-layer mantle model comparable with ours. The results shown in our figures suggest, in agreement with the conclusions from RSL data, that the different viscosity models obtained in the past are mainly a consequence of a different way of mantle stratification.

6. Conclusions

A completely analytical scheme based on the normal mode technique has been applied for the first time to model the isostatic and rotational response to the Pleistocene deglaciation of a multilayered Earth based on PREM. Our procedure assures the accurate detection of the inverse relaxation times and corresponding residues. The 31-layer models are sufficient for both TPW and $\dot{J}_2$ to reach the continuum limit in the sense that further increase in the number of layers and refinement toward a continuous variation of the density profile with respect to PREM is not visible in polar wander nor in the variation of the degree 2 component of the geopotential.

For an upper mantle viscosity varying between 10^{20} and 10^{21} Pa s the shape of the TPW and $\dot{J}_2$ curves as a function of the viscosity of the lower mantle agrees with both previous analytical results based on simplified mantle models [*Yuen and Sabadini*, 1984; *Spada et al.*, 1992] and recent findings by *Milne and Mitrovica* [1996]. The TPW curves show a nonmonotonic decrease in the signal from about $3°$ Myr^{-1} for an isoviscous mantle to zero for lower mantle viscosities higher than 10^{23} Pa s, with a characteristic upwarping in proximity of 10^{22} Pa s. The local maximum in TPW simulations is responsible for a multiplicity of solutions in the inference of lower mantle viscosity from 3×10^{21} to 10^{22} Pa s. These findings are in distinct contrast with recent analyses by *Peltier and Jiang* [1996], who, for viscosity contrasts located at 670 km, predict that TPW is negligible in the proximity of 10^{22} Pa s, where our local maximum of $0.9°$ Myr^{-1} is located. There are indications that *Peltier and Jiang's* [1996] results are affected by internal inconsistencies, although more precise conclusions would require knowledge of TPW and $\dot{J}_2$ values in a viscosity range not shown by *Peltier and Jiang* [1996].

When the depth of the viscosity contrast is increased from 670 km to 1471 km in the lower mantle, the multiplicity of solutions for both TPW and $\dot{J}_2$ in the inference of the viscosity of the lowermost portion of the mantle disappears. In the TPW curve this occurs via a reduction in the local maximum at 10^{22} Pa s at a sin-

gle crossing of the observational data, while in $\dot{J}_2$ the high-branch viscosity solution disappears because of an increase in the signal beyond -3×10^{-11} yr^{-1} for viscosities in the lowermost mantle higher than 3×10^{21} Pa s. If the viscosity contrast is located at depths of about 1400 km, TPW and $\dot{J}_2$ data allow for an unambiguous viscosity solution for the upper portion of the mantle of 10^{21} Pa s, agreeing with *Haskell*'s [1935] viscosity. This result agrees well with the findings by *Mitrovica* [1996], who, on the basis of an accurate analysis on the resolving power of Frechet integrals for RSL data, demonstrated that the value of 10^{21} Pa s first proposed by *Haskell* [1935] should not be considered limited to the upper mantle but rather to the upper 1000-1400 km of the whole mantle. Our results reinforce this interpretation, indicating that what *Mitrovica* [1996] found for relative sea levels is also valid for rotational and geopotential signatures. A viscosity of 10^{21} Pa s limited to the upper mantle has been retrieved in some previous TPW and $\dot{J}_2$ analyses because of the underestimate of the mantle buoyancy of simplified five-layer fixed boundary contrast models and of the trade-off between the density and the viscosity profile [e.g., *Spada et al.*, 1992].

If the viscosity contrast is located at 670 km depth, which defines the boundary between the upper and the lower mantles based on seismological data, TPW and $\dot{J}_2$ indicate a clear trend toward viscosities in the upper mantle lower than the *Haskell* value of 10^{21} Pa s. This increases the viscosity contrast to a factor of 20, in agreement with the far field RSL analysis by *Lambeck et al.* [1990] and with the studies on the long-wavelength geoid anomalies supported by mantle convection [*Richards and Hager*, 1984]. When analytical stratified models carrying all the buoyancy of PREM are considered, it becomes possible to explain some apparently contradictory results of recent inferences of mantle viscosity.

References

Besse, J., and V. Courtillot, Revised and synthetic apparent polar wander paths of the African, Eurasian, North American, and Indian Plates, and true polar wander since 200 Ma, *J. Geophys. Res., 96*, 4029-4050, 1991.

Bills, B. G., and T. S. James, Polar motion of a viscoelastic Earth due to glacial cycle mass loading, *J. Geophys. Res., 102*, 7579-7602, 1997.

D'Agostino, G., G. Spada, and R. Sabadini, A semi-analytical approach for a laterally varying viscoelastic mantle, *Geophys. J. Int., 129*, F1-F5, 1997.

Devoti, R., M. Fermi, V. Luceri, P. Rutigliano, C. Sciarretta and G. Bianco, Estimation of low degree geopotential coefficients using SLR data, *Annales Geophysicae, 15(I), Supplement I*, C126, 1997.

Dickman, S. R., Secular trend of the Earth's rotation pole: Consideration of motion of the latitude observatories, *Geophys. J. R. Astron. Soc., 51*, 229-244, 1977.

Dziewonski, A. M., and D. L. Anderson, Preliminary reference Earth model, *Phys. Earth Planet. Inter., 25*, 297-356, 1981.

Forte, A. M., and J. X. Mitrovica, New inferences of mantle viscosity from joint inversion of long-wavelength mantle convection and post-glacial rebound data, *Geophys. Res. Lett., 23*, 1147-1150, 1996.

Han, D., and J. M. Wahr, The viscoelastic relaxation of a realistically stratified Earth, and a further analysis of postglacial rebound, *Geophys. J. Int., 120*, 287-311, 1995.

Haskell, N. A., The motion of a fluid under a surface load, *Physics, 6*, 265-269, 1935.

James, T. S., and E. R. Ivins, Global geodetic signatures of the Antarctic ice sheet, *J. Geophys. Res., 102*, 605-633, 1997.

Lambeck, K., *The Earth's Variable Rotation: Geophysical Causes and Consequences*, Cambridge Univ. Press, New York, 1980.

Lambeck, K., P. Johnston, and M. Nakada, Holocene glacial rebound and sea-level change in NW Europe, *Geophys. J. Int., 103*, 451-468, 1990.

Lambeck, K., P. Johnston, C. Smither, and M. Nakada, Glacial rebound of the British Isles - III, Constraints on mantle viscosity, *Geophys. J. Int., 125*, 340-354, 1996.

McCarthy, D. D., and B. J. Luzum, Path of the mean rotational pole from 1899 to 1994, *Geophys. J. Int., 125*, 623-629, 1996.

Milne, G. A., and J. X. Mitrovica, Post-glacial sea level change on a rotating Earth: First results from a gravitationally self-consistent sea-level equation, *Geophys. J. Int., 126*, F13-F20, 1996.

Mitrovica, J. X., Haskell [1935] revisited, *J. Geophys. Res., 101*, 555-569, 1996.

Mitrovica, J. X., and A. M. Forte, Radial profile of mantle viscosity: Results from the joint inversion of convection and postglacial rebound observables, *J. Geophys. Res., 102*, 2751-2769, 1997.

Mitrovica, J.X., and G. A. Milne, Glaciation-induced perturbations in the Earth's rotation: A new appraisal, *J. Geophys. Res.*, in press, 1997.

Mitrovica, J. X., and W. R. Peltier, Present-day secular variations in the zonal harmonics of the Earth's geopotential, *J. Geophys. Res., 98*, 4509-4526, 1993.

Mitrovica, J. X., A. M. Forte, and R. Pan, Glaciation-induced variations in the Earth's precession frequency, obliquity and insolation over the last 2.6 Ma, *Geophys. J. Int., 128*, 270-284, 1997.

Munk, W. H., and G. F. MacDonald, *The Rotation of the Earth*, Cambridge Univ. Press, New York, 1960.

Nakada, M., and K. Lambeck, Late Pleistocene and Holocene sea-level change in the Australian region and mantle rheology, *Geophys. J. Int., 96*, 497-517, 1989.

Nakiboglu, S. M., and K. Lambeck, Deglaciation effects on the rotation of the Earth, *Geophys. J. R. Astron. Soc., 62*, 49-58, 1980.

Peltier, W. R., The LAGEOS constraint on deep mantle viscosity: Results from a new normal mode method for the inversion of viscoelastic relaxation spectra, *J. Geophys. Res., 90*, 9411-9422, 1985.

Peltier, W. R., and X. Jiang, Glacial isostatic adjustment and Earth rotation: Refined constraints on the viscosity of the deepest mantle, *J. Geophys. Res., 101*, 3269-3290, 1996.

Ricard, Y., R. Sabadini, and G. Spada, Isostatic deformations and polar wander induced by internal mass redistribution, *J. Geophys. Res., 97*, 14223-14236, 1992.

Ricard, Y., G. Spada, and R. Sabadini, Polar wandering of a dynamic Earth, *Geophys. J. Int., 113*, 284-298, 1993.

Richards, M. A., and B. H. Hager, Geoid anomalies in a dynamic Earth, *J. Geophys. Res., 89*, 5987-6002, 1984.

Sabadini, R., and W. R. Peltier, Pleistocene deglaciation and the Earth's rotation: Implications for mantle viscosity, *Geophys. J. R. Astron. Soc., 66*, 553-578, 1981.

Sabadini, R., D. A. Yuen, and E. Boschi, Polar wandering and the forced responses of a rotating, multilayered, viscoelastic planet, *J. Geophys. Res., 87*, 2885-2903, 1982.

Sabadini, R., D. A. Yuen, and E. Boschi, A comparison of the complete and truncated versions of the polar wander equations, *J. Geophys. Res., 89*, 7609-7620, 1984.

Sabadini, R., D. A. Yuen, and P. Gasperini, Mantle rheology and satellite signatures from present-day glacial forcings, *J. Geophys. Res., 93*, 437-447, 1988.

Sabadini, R., D. A. Yuen, and R. Widmer, Constraints on short-term mantle rheology from the $\dot{J}_2$ observation and the dispersion of the 18.6 y tidal Love number, *Phys. Earth Planet. Inter., 38*, 235-249, 1985.

Spada, G., R. Sabadini, D. A. Yuen, and Y. Ricard, Effects on post-glacial rebound from the hard rheology in the transition zone, *Geophys. J. Int., 109*, 683-700, 1992.

Steinberger, B., and R. J. O'Connell, Changes of the Earth's rotation axis owing to advection of mantle density heterogeneities, *Nature, 387*, 169-173, 1997.

Tushingham, A. M., and W. R. Peltier, ICE-3G: A new global model of late Pleistocene deglaciation based upon geophysical predications of postglacial relative sea level change, *J. Geophys. Res., 96*, 4497-4523, 1991.

Tushingham, A. M., and W. R. Peltier, Validation of the ICE-3G model of Würm-Wisconsin deglaciation using a global data base of relative sea level histories, *J. Geophys. Res., 97*, 3285-3304, 1992.

Vermeersen, L.L.A., Changes in the Earth's Rotation by Tectonics: Gravito-elastodynamics, Ph.D.-thesis, Utrecht University, Utrecht, Netherlands, 1993.

Vermeersen, L. L. A., and R. Sabadini, Significance of the fundamental mantle rotational relaxation mode in polar wander simulations, *Geophys. J. Int., 127*, F5-F9, 1996.

Vermeersen, L. L. A., and R. Sabadini, A new class of stratified viscoelastic models by analytical techniques, *Geophys. J. Int., 129*, 531-570, 1997.

Vermeersen, L. L. A., and N. J. Vlaar, Changes in the Earth's rotation by tectonic movements, *Geophys. Res. Lett., 20*, 81-84, 1107-1109, 1993.

Vermeersen, L. L. A., R. Sabadini, G. Spada, and N. J. Vlaar, Mountain building and Earth rotation, *Geophys. J. Int., 117*, 610-624, 1994.

Vermeersen, L. L. A., R. Sabadini, and G. Spada, Analytical visco-elastic relaxation models, *Geophys. Res. Lett., 23*, 697-700, 1996a.

Vermeersen, L. L. A., R. Sabadini, and G. Spada, Compressible rotational deformation, *Geophys. J. Int., 126*, 735-761, 1996b.

Wu, P., and W. R. Peltier, Pleistocene deglaciation and the Earth's rotation: A new analysis, *Geophys. J. R. Astron. Soc., 76*, 753-791, 1984.

Yoder, C. F., J. G. Williams, J. O. Dickey, B. E. Schutz, R. J. Eanes, and B. D. Tapley, Secular variation of the Earth's gravitational harmonic J_2 coefficient from Lageos and non tidal acceleration of Earth rotation, *Nature, 303*, 757-762, 1983.

Yuen, D. A., and R. Sabadini, Secular rotational motions and the mechanical structure of a dynamical viscoelastic Earth, *Phys. Earth. Planet. Inter., 36*, 391-412, 1984.

Yuen, D. A., R. Sabadini, P. Gasperini, and E. Boschi, On transient rheology and glacial isostasy, *J. Geophys. Res., 91*, 11420-11438, 1986.

A. Fournier, Departement des Sciences de la Matiere, ENS Lyon, 46 Allee d'Italie, F-69364 Lyon Cedex 7, France. (e mail: afournie@ens.ens-lyon.fr)

R. Sabadini, Dipartimento di Scienze della Terra, Sezione Geofisica, Università di Milano, Via Cicognara, 7, 20129 Milano, Italy. (e-mail: bob@sabadini.geofisica.unimi.it)

L. L. A. Vermeersen, Geodetic Institute, Stuttgart University, Geschw-Scholl-Strasse 24D, D-70174 Stuttgart, Germany. (e-mail: vermeer@gis.uni-stuttgart.de)